JOURNAL OF Applied Polymer SCIENCE

Synthesis of Urethane Acrylate based Electromagnetic Interference Shielding Materials

Meltem Yanılmaz,[1] Betül Türel Erbay,[2] Ersin Serhatli,[2,3] Abdulkadir Sezai Sarac[2,3]

[1]Textile Engineering, Faculty of Textile Technology and Design, Istanbul Technical University, Taksim, Istanbul 34437, Turkey
[2]Polymer Science and Engineering, Institute of Science and Technology, Istanbul Technical University, Maslak, Istanbul 34469, Turkey
[3]Department of Chemistry, Faculty of Science and Letters, Istanbul Technical University, Maslak, Istanbul 34469, Turkey
Correspondence to: A. S. Sarac (E-mail: sarac@itu.edu.tr)

ABSTRACT: In this work, a new method, consists of synthesis of urethane acrylate (UA) followed by *in situ* polymerization of pyrrole using cerium (IV) as an oxidant and UV-curing of the composites, for preparing polypyrrole–UA (PPy–UA) composite films was described. It appeared that dielectric constants of the composites increased with increasing the PPy content and decreased with increasing the frequency from 10^{-2} to 10^{7}, indicating an interfacial Maxwell–Wagner contribution to the permittivity. An incorporation of a small amount of PPy (15% Py) to UA matrix increased their dielectric constants more than 4×10^{4} (41,259) at 10^{-2} Hz. So, the incorporation of PPy was very effective for enhancing the dielectric properties of UA matrix. Furthermore, the significant enhancement in dielectric properties (loss tangent and dielectric constant) contributes to the improvement in electromagnetic interference shielding efficiency. Composite films were characterized using Fourier transform infrared attenuated total reflectance (FTIR-ATR) spectrophotometer and ^{1}H-NMR. It was seen that PPy is blended with the UA matrix at the molecular level through H-bonding interactions. A linear relationship was also observed between the characteristic groups' absorbances of PPy (from FTIR-ATR) and dielectric constant values (from dielectric spectrometer). © 2012 Wiley Periodicals, Inc. J. Appl. Polym. Sci. 000: 000–000, 2012

KEYWORDS: polypyrrole; urethane acrylate; composite; FTIR-ATR

Received 9 February 2012; accepted 17 May 2012; published online
DOI: 10.1002/app.38094

INTRODUCTION

Because of its unique properties, polypyrrole (PPy) has been studied for many applications such as antistatics, electromagnetic shielding, actuators, and polymer batteries. However, the high degree of conjugation in the molecular backbone of PPy makes it very rigid, insoluble, and poorly processable. It is, therefore, very difficult to use it alone as a structural material. Processing conducting polymers in form of blends and composites with commercial polymers is a well-established alternative as a material for technological applications. Moreover, the assessment of any eventual modification of the original physical properties in the compound material due to the interaction between its constituents is also highly desirable in any scientific investigation of a blend or a composite.[1–4] In recent years, a variety of PPy composites have been studied using many types of synthetic polymers such as poly(methyl methacrylate), polyvinylchloride, polystyrene, and polyurethane (PU).[5–8]

PU, used in diverse industrial applications, is an important coating material due to its superior physical properties and great versatility. The physical properties of PU are derived from their molecular structure caused by interactions between the polymer chains. The segmental flexibility, the chain entanglement, and the cross-linkage influence the properties and determine the use of the end products. To improve its properties, PU-based composites has received increasing interests. Among the oligomers used for UV-curable coatings, urethane acrylate (UA) oligomers offer the best mechanical and chemical properties, such as high impact and tensile strength, high functionality, superior abrasion resistance, desirable toughness, and excellent resistance to chemicals and solvents combined with faster and easier process.[9–15]

Besides providing valuable information with respect to morphology and phase changes, molecular structure, polarization, dipole motions, and their mutual influence on the properties of the material, the relaxed dielectric constant (ε'), which is especially important to determine dipolar correlations, as well as, the dielectric strength of relaxation processes, can be obtained using dielectric spectroscopy. In earlier publications,[16] it has been shown that the increase in the dielectric permittivity is a key factor for increasing the energy conversion. Among the various ways to raise the dielectric permittivity, the development of polymeric composites is of interest. The electrical properties are

directly related to the permittivity and conductivity, which strongly depend on the dispersion of the second component throughout the polymer matrix as well as on the effective microstructure of the composite.[17]

The reflection and/or adsorption of electromagnetic radiation by a material is referred to as electromagnetic interference (EMI) shielding, and the material acts as a shield against the penetration of radiation. The EMI shielding efficiency (SE) of a composite material is effected by the filler's intrinsic conductivity, dielectric constant, and aspect ratio. It is well known from previous studies that EMI shielding efficiency is proportional to the conductivity as well as the permittivity of a material.[18–22]

We previously reported the synthesis of conductive PU–PPy composite films and nanofibers.[23,24] In this study, our approach is to combine PPy with UA in the goal of generating a novel coating material with enhanced dielectric properties. The feasibility of preparing a PPy–UA composite with a low PPy content is demonstrated, and the dielectric properties of the composites are investigated. The dielectric data obtained for PPy–UA polymeric material are also analyzed to investigate and correlate the effect of PPy on the UA matrix. In addition to dielectric measurements, determinations with Fourier transform infrared (FTIR)-ATR spectrophotometer and ^{1}H-NMR have been performed to investigate how the microstructure of the composite is affected by adding PPy in UA matrix. It is seen that PPy is blended with the UA matrix at the molecular level through H-bonding interactions. It may be due to some kind of interaction such as hydrogen bonding between PPy and UA chains.

EXPERIMENTAL

Materials

Dibutyltin dilaurate (DBTDL) was purchased from Air Products (Allentown, PA). Isophorone diisocyanate (Desmodur I) was supplied from Bayer (Istanbul, Turkey). Polypropylene glycol (PPG; Lupranol 1100; M_w = 1100 g mol^{-1}) was supplied from Elastogran, BASF (Istanbul, Turkey). PPG was placed in a vacuum oven at 80°C for 8 h before carrying out the reaction. Also, 2-hydroxyethyl methacrylate (HEMA) from Laporte Performance Chemicals (Hythe, UK), dipropyleneglycol diacrylate (DPGDA) from CYTEC Chemicals (Woodland, NJ), Irgacure 184 (1-hydroxy-cyclohexyl-phenyl-ketone) from Ciba Chemicals (Basel Switzerland), and 1,6-hexanediol diacrylate (HDDA) from Sartomer Chemicals (Exton, PA) were used for preparing films. Acetone (Acn, Aldrich and Merck, analytical) and *N*-Vinyl pyrrolidinone (NVP, Aldrich (Taufkirchen, Germany), analytical) were used as solvents. Pyrrole (Py) (C_4H_5N; Aldrich, analytical) and ceric ammonium nitrate (CAN) $(NH_4)_2[Ce(NO_3)_6]$, BDH Middle East L.L.C. (Dubai, UAE) analytical) were used. All reagents (98% purity) were used without further purification.

Experimental Methods

The alternating current conductivity measurements were carried out using a Novocontrol Broadband Dielectric Spectrometer (Alpha-a high-performance frequency analyzer, frequency domain 0.001–3 GHz) at 25°C. The sample was prepared for the dielectric measurement as thin film between two-gold circular disks (diameter = 2 cm) as electrodes. The cell is placed inside a cryostat. FTIR-ATR analysis of composite films was carried out by FTIR reflectance spectrophotometer (Perkin Elmer, Spectrum One, with a Universal ATR attachment with a diamond and ZnSe crystal). ^{1}H-NMR measurement was conducted on a Bruker 250 MHz Spectrometer at room temperature using deuterated dimethyl sulfoxide (DMSO) (DMSO-d_6) as the solvent. Tetramethylsilane (TMS) was used as internal standard. The free films were prepared using a Teflon mold (100 × 100 × 1 mm^3). The glass transition temperatures (T_g) were obtained by differential scanning calorimetry (DSC) on a Thermal Analysis TA Ins. DSC Q10; 2–3 mg of UA was initially heated under nitrogen from −80 to 350°C at a rate of 10°C min^{-1}, and the T_g values were obtained following rapid cooling, from a second heating at the same heating rate. Thermogravimetrical analysis (TGA) was carried out on a TA TGA Q50 from 20 to 700°C at a heating rate of 20°C min^{-1} in nitrogen.

Synthesis of UA

UA was prepared by a two-step solution polymerization method. In the first step, the prepolymer was synthesized from PPG (0.02 molequiv.) and isophorone diisocyanate (0.04 molequiv.) at an [OH]/[NCO] ratio of 1 : 2 in a 100 mL, round-bottom three-necked reaction kettle equipped with a magnetic stirrer, heating mantle, reflux condenser, dropping funnel, nitrogen inlet, and $CaCl_2$ tube. PPG was dissolved in acetone, and isophorone diisocyanate (IPDI) dissolved in acetone was fed dropwise over 30 min into the reactor. The dibutyltin dilaurate (DBTDL) was added as a catalyst, and the temperature was increased to 55°C. The reaction was continued till the NCO content reached the theoretical value as determined by dibutylamine titration. In the second step, HEMA (0.04 molequiv.) was added over 30 min to the mixture of the prepolymer to provide [OH]/[NCO] ratio of 1 : 1. The temperature was maintained at about 50°C to allow the termination to take place. The reaction was continued until NCO peak at 2270 cm^{-1} disappeared totally in the FTIR-ATR spectra of samples taken from the reaction medium every 0.5 h. The final product was vacuum dried at ambient temperature. We used earlier studies[25–27] to synthesize UA. The reactions take place according to Scheme 1.

The FTIR spectrum of UA is shown in Figure 1. In the spectrum the characteristic peaks of N—H (3340 cm^{-1}), and —C=O (1715 cm^{-1}), —C—H aliphatic stretching bands (2970–2870 cm^{-1}) are also observed. The band at 1530 cm^{-1} verified the formulation of O—CO—NH stretching groups. The characteristic peak of acrylate (CH_2=C—) is detected at 1638 cm^{-1}. The absorption band at 1100 cm^{-1} originates from C—O—C group. The disappearance of the absorption bands of the NCO group (2270 cm^{-1}) of IPDI and OH groups also indicates that isocyanatoes entirely reacted. After the curing reaction in the IR spectrum the absorption of double bond (CH_2=C—) at 1638 cm^{-1} disappears. Thus, the double bonds of the UA polymerized.[28]

Figure 2 shows ^{1}H-NMR spectra of UA in DMSO-d_6. The peaks at 0.78–1.20 ppm are ascribed to the methyl (CH_3) protons and CH_2 protons of IPDI and methyl protons of PPG. CH_2 protons in the cyclic ring of IPDI were at δ = 1.20–1.7 ppm. The peaks in the range of 1.80–2.00 ppm are methyl protons of HEMA. The peaks at 2.90–4.20 ppm are ascribed to the CH and CH_2

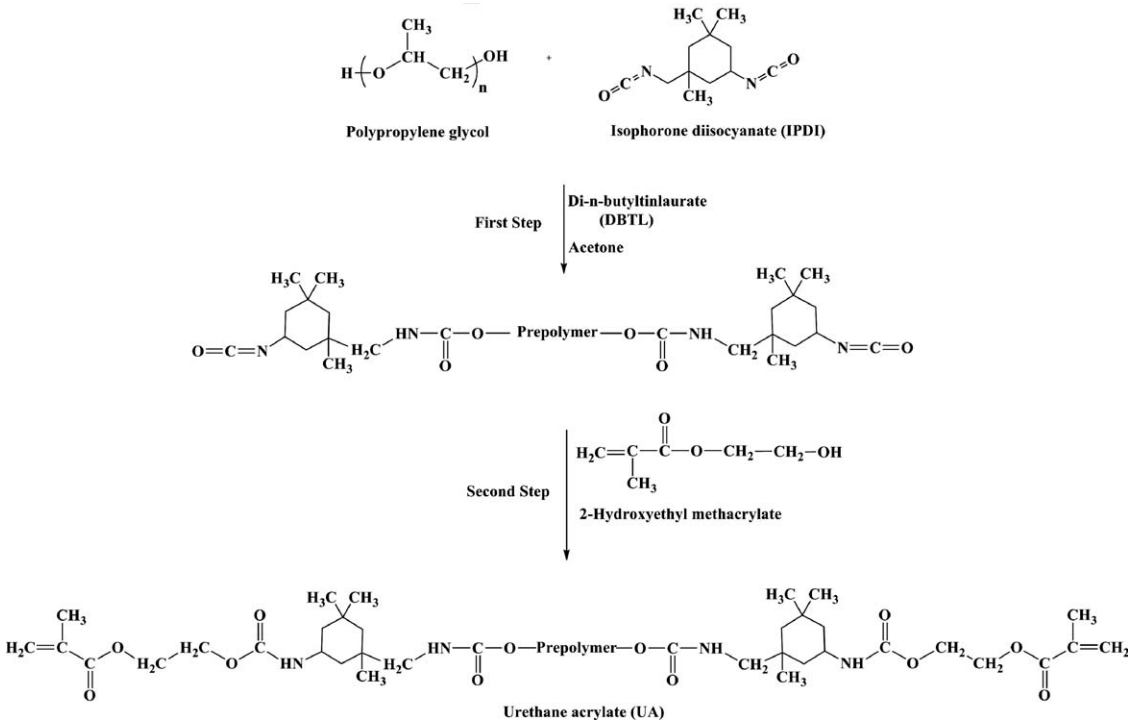

Scheme 1. Synthesis of UA.

protons of IPDI (NCOCH and $NCOCH_2$), CH_2 protons of HEMA ($O(CH_2)_2OCO$). The peaks in the range of 5.50–5.70 and 5.90–6.10 ppm are obviously observed, which prove the existence of acrylic group in UA structure related with HEMA. The peaks at 6.9–7.3 ppm are ascribed to the protons of —NH— groups in urethane unit. DSC measurements were conducted with a heating rate of 10°C min^{-1}. In all cases, the T_g could be easily measured in the second heating traces of DSC. The T_g value of the UA was in the range of (−48)–(−55)°C.

Preparation of PPy–UA Composite Films

The coating formulations were mixed of UA, HDDA, DPGDA, and NVP that are used as reactive diluents and Irgacure 184 as photoinitiator. The formulation can be seen in Table I.

UA as reactive oligomer and DPGDA, HDDA, and NVP as reactive diluents first mixed for 15 min to obtain a homogeneous mixture, and then Py was added into the acrylate matrix. After

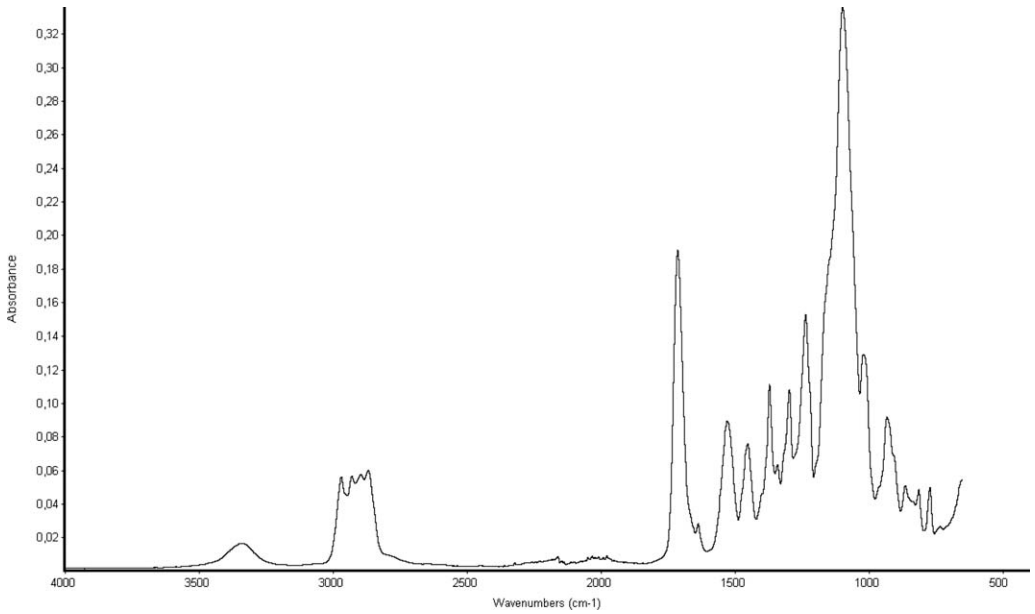

Figure 1. FTIR ATR spectrum of UA.

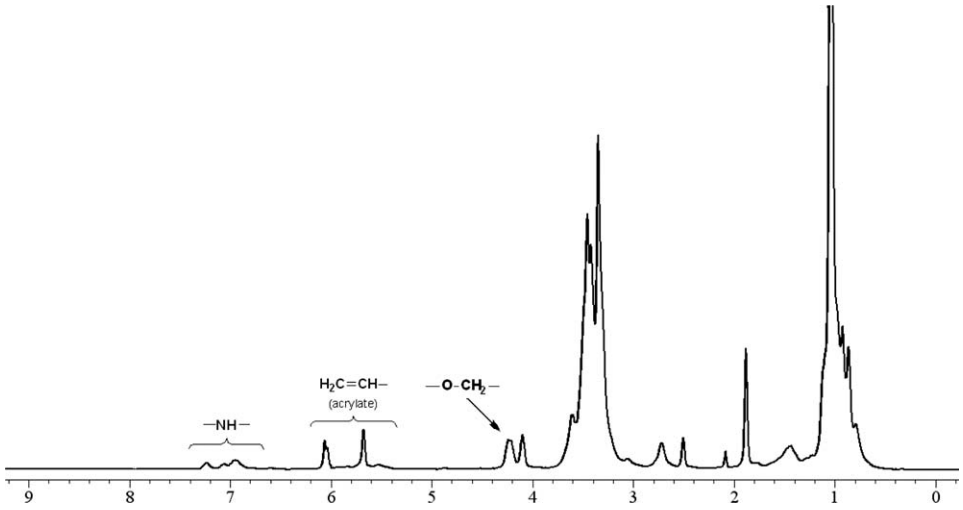

Figure 2. ^{1}H-NMR spectrum of UA.

stirring for 1 h to obtain homogeneous mixture, Ce(IV) was used to polymerize Py on UA matrix. The weight percentages of Py (Py/(UA: 5%, 10%,15%) were calculated and reported using the initial weight of UA component. After the reaction was completed (2 h), the photoinitiator (Irgacure-184) was added to the UA-Py matrix.

After homogenization, free films were prepared by pouring the liquid on to a Teflon mold. Transparent polyester film was covered on to the Teflon mold to obtain a smooth surface. The films situated 10 cm above the Teflon mold under UV-lamp (OSRAM, 300 W) were obtained after 180 sec irradiation. The thicknesses of films are about 0.25 mm. Preparation of PPy–UA composites can be seen in Scheme 2.

Experimental Methods

The alternating current conductivity measurements were carried out using a Novocontrol Broadband Dielectric Spectrometer (Alpha-a high-performance frequency analyzer, frequency domain 0.001–3 GHz) at 25°C. The sample was prepared for the dielectric measurement as thin film between two-gold circular disks (diameter = 2 cm) as electrodes. The cell is placed inside a cryostat. FTIR-ATR analysis of composite films was carried out by FTIR reflectance spectrophotometer (Perkin Elmer, Spectrum One, with a Universal ATR attachment with a diamond and ZnSe crystal). ^{1}H-NMR measurement was conducted on a Bruker 250 MHz Spectrometer at room temperature using deuterated DMSO as the solvent. TMS was used as internal standard.

Table I. UA Formulation

Components	Formulation (wt %)
UA	50
DPGDA	37
HDDA	10
Photoinitiator (I-184)	3

RESULTS AND DISCUSSION

FTIR-ATR and ^{1}H-NMR Study

Figure 3 shows the FTIR-ATR spectra of the UA films with and without PPy. FTIR-ATR spectra of UA and PPy–UA composites show the following absorption: 3280–3362 cm^{-1} of N—H stretching, 2800–2933 cm^{-1} of C—H stretching, 1715 cm^{-1} of C=O stretching, 1531 cm^{-1} of N—C=O and NH^{δ}, 1090 cm^{-1} of —O— stretching bond. The characteristic absorption band at ~3330 cm^{-1} indicates the stretching of hydrogen bonding of N—H band. The bands at 1729 cm^{-1} (amide I, νC= O), 1536 cm^{-1} (amide II, δN—H and νC—N), 1240 cm^{-1} (amide III, νC—N and δN—H) and 1114 cm^{-1} (antisymmetric νC—O—C) confirm the formation of urethane group. The inset figure of Figure 3 shows the absorbance increases of CH in plane vibration (1291 cm^{-1})[29] and CN stretching vibration (1446 cm^{-1})[29–31] versus Py content. PPy addition in UA matrix leads to significant increases in the characteristic absorbances of PPy. This observation indicates PPy inclusion into matrix.

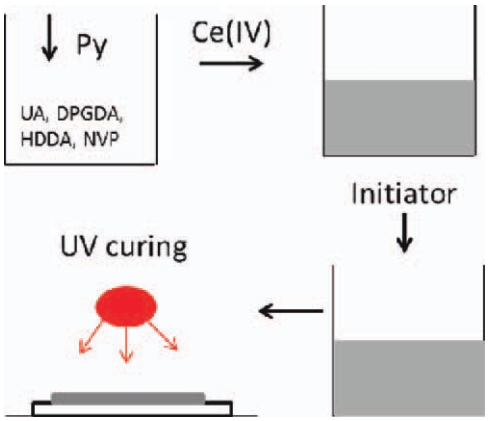

Scheme 2. Schematic illustration of the composite films preparation process. [Color figure can be viewed in the online issue, which is available at wileyonlinelibrary.com.]

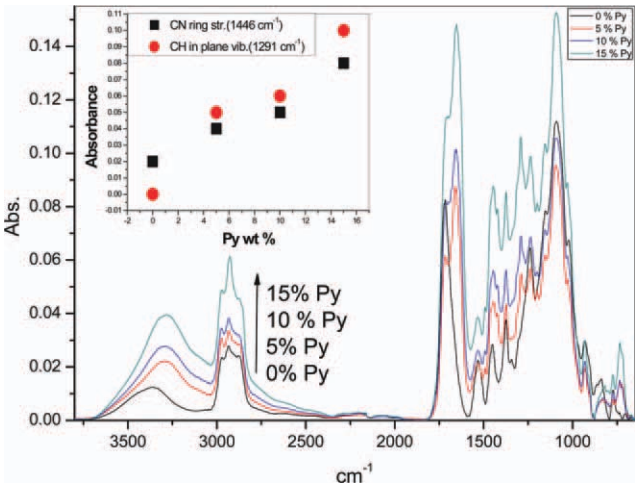

Figure 3. The FTIR ATR spectra of UA and PPY–UA composites (inset: increase of the absorbances of PPy vs. Py content). [Color figure can be viewed in the online issue, which is available at wileyonlinelibrary.com.]

In determining the morphology and other properties of PUs, hydrogen bonding plays very critical roles due to medium to strong hydrogen bonding interactions between amide urethane urea groups.[32] Oprea et al.[33] indicated that participation in hydrogen bonding decreases the frequency of the NH vibration and increases its intensity, making this absorption useful in the study of hydrogen-bond effects. The FTIR-ATR spectra for composites show a shifting of hydrogen bonded —NH groups absorption peak toward the lower wavenumber region (from 3362 to 3281 cm^{-1}). The shifting of absorption peak also indicates the interaction between UA and PPy due to hydrogen bonding or another term the shift of the hydrogen bonded —NH groups indicates that the hydrogen bonding effect is more pronounced with adding of PPy.

A new peak appear at 1652 cm^{-1} is observed for the PPy–UA films, which does not appear in the UA matrix, and the intensity of the peak was increased due to adding Py. The absorption peak arise at 1652 cm^{-1} referred to the amide (HN—C=O) group stretching vibration.[34] It indicates the presence of H-bonding between C=O groups of UA and NH groups of PPy. Schemes 3 and 4 show the H-bonding between UA matrix and PPy.

The region of 1780–1600 cm^{-1} is related to C=O stretching mode, and multiple peaks in this region reflect the complex properties of hydrogen bonding. Barick and Tripathy[35] prepared PU carbon nanotube composites and reported similar results. The stretching band of 1652 cm^{-1} increases with increase in wt % of multiwalled carbon nanotube (MWNT) loading due to the physical adhesion caused by the hydrogen bond between both the —NH and the >C=O groups of the TPU matrix and MWNTs.[35]

According to Sung and Schneider,[36] the two —C=O absorptions at 1715 and 1652 cm^{-1} were assigned to be disordered and ordered bonded carbonyl absorptions, respectively. The capability of the —C=O groups to bond with the —NH groups would interfere with a regular packing. According to FTIR-ATR spectra comparison, adding PPy in UA matrix leads to regular packing due to H bonding between —C=O of urethane and —NH of PPy. In Figure 4, the linear relationship between the absorbances of C=O str (1652 cm^{-1}) and the dielectric constant values of the composites can be seen. An increase in Py content leads to increase in the absorbance and dielectric constant values. It indicates Py polymerization on UA matrix.

The FTIR-ATR spectra of PPy–UA show absorption bands centered at 3362 cm^{-1}, which is characteristic of urethane —NH stretching frequencies. This broadening band with increasing PPy content indicates a strong and unique kind of H-bond as further supported by ^{1}H-NMR spectroscopy. A sharp increase in 2.08 ppm for PPy–UA composites can be seen in Figure 7. Similar result for detecting H bonding were reported by Lu et al.[37] The signals from 2 to 2.5 ppm is characteristic for urethanic groups.[38] The peak at 4.8–5 ppm was due to the —NH— protons of Py. The intensities of the peaks increased with the

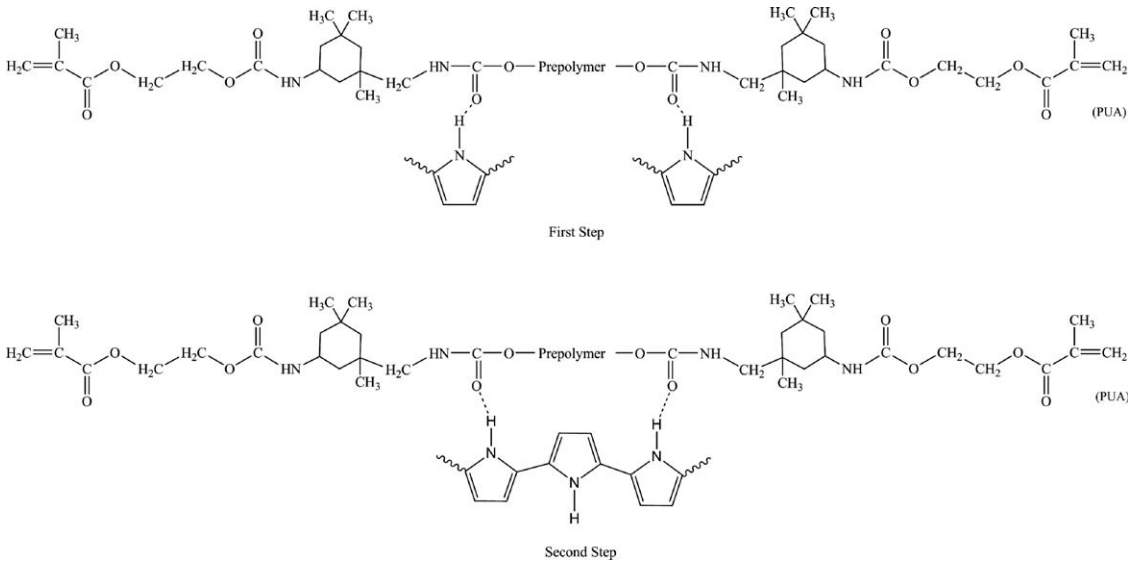

Scheme 3. First and second step of H-bonding formation.

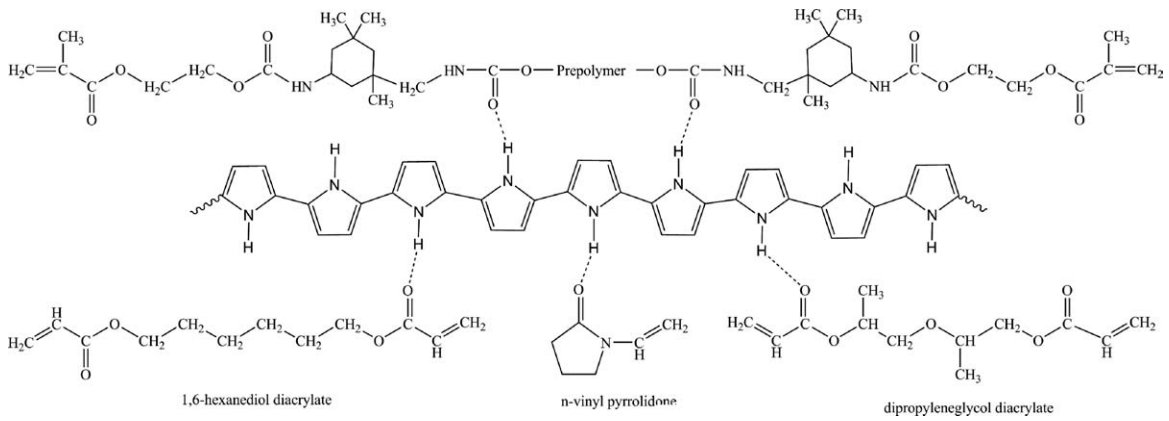

Scheme 4. General view of H-bonding formation.

increase of the Py content in the UA system and are shown in Figure 5. The peaks in the range of 5.67–6.05 ppm are obviously observed in spectra, which prove the existence of acrylic group in UA molecular structure related with HEMA. The peaks at 6.9–7.2 ppm are ascribed to the protons of urethanic —NH— groups in urethane unit.

Dielectric Spectroscopy Study

The dielectric data have been analyzed and discussed using two functions of the dielectric spectroscopy; the dielectric function ε^* ($\varepsilon^* = \varepsilon' - i\varepsilon''$) and the electric modulus M^* ($M^* = M' + iM''$). The dielectric function ε^* is used to describe the dielectric behavior (polarization mechanisms) of the materials, and the electric modulus M^* is used to describe the electrical behavior (conductivity relaxation mechanisms) of the materials. The loss factor ($\tan\delta = \varepsilon''/\varepsilon' = M''/M'$) gives directly the phase difference due to the absorption of energy.[39,40]

The mole ratio of monomer to oxidant is a crucial factor for the preparation of PPy with good conductivity.[41] To determine the most appropriate oxidant per monomer molar ratio with the aim of obtaining the highest dielectric properties, the samples with different [Ce(IV)/Py] ratios were prepared. Figure 6 shows the

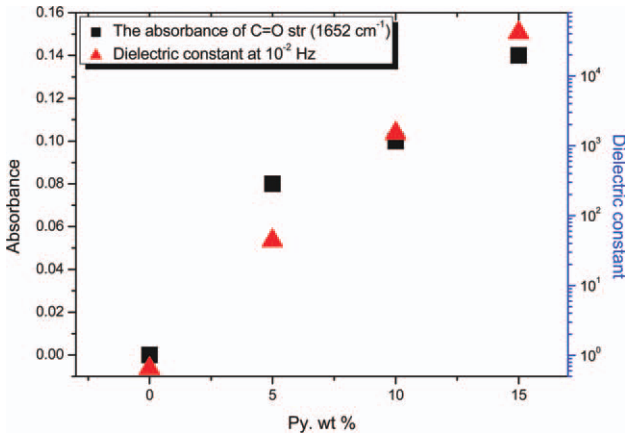

Figure 4. The relationship between the absorbance of C=O str and dielectric constant values. [Color figure can be viewed in the online issue, which is available at wileyonlinelibrary.com.]

dielectric constants and M'' plots versus frequency for the UA matrix and the composite samples prepared with different [Ce(IV)/Py] ratios. As it is shown in Figure 6, the sample with the ratio ([Ce(IV)/Py]=)1/27 has the highest dielectric constant (~1500). After determining the [Ce(IV)/Py] ratio, Py wt % was increased in the samples to obtain better dielectric properties and to investigate the effect of PPy content on the dielectric characteristics. The pictures (magnitude 1×) of the films can be seen on the right side of Figure 6 to show color differences between films.

In Figure 7, the dependence of the dielectric constant on the frequency for UA and PPy–UA composites is shown. It is observed significantly that the PPy–UA composites show a polar character in contrast to a nonpolar UA matrix. In the inset plot of Figure 7, a significant increase in dielectric constant (at 10^{-2} Hz) as a function of Py content can be seen. The dielectric constant of the samples increases with an increase of PPy content. It is due to the fact that PPy has high dielectric molecules. It is very interesting that an incorporation of a small amount of PPy to UA matrix increases dielectric constant of UA matrix more than 4×10^3 at 10^{-2} Hz. The dielectric constant of PPy–UA composites with 15 wt % Py at 10^{-2} Hz is 41259, whereas that of the neat UA is about 1. So, it is sure that the incorporation of PPy is very effective for enhancing the dielectric properties of samples. In the plot of log ε' versus log f, a mechanism of dielectric losses is shifted to higher frequencies as PPy content increases. In the first frequency region that is between 10^{-2} and 10 Hz, sharp decrease relaxations processes are observed due to charge accumulation in different interspaces. These processes are attributed to Maxwell–Wagner–Sillars interfacial polarization.[42] This polarization contributed to the increase in the permittivity constant value versus PPy content—an observation that was in good agreement with the assumed power law (1)

$$\varepsilon = \varepsilon_i |(f_c - f)/f_c|^{-q} \quad (1)$$

where ε_i is the dielectric constant of the polymer matrix, q is a critical exponent, f_c is the percolation threshold for the conduction, and f is the volume fraction of the second component in the composites. In our case,

$$\varepsilon_{PPy-UA} = \varepsilon_{UA} |(f_c - f_{Py\%})/f_c|^{-q}$$

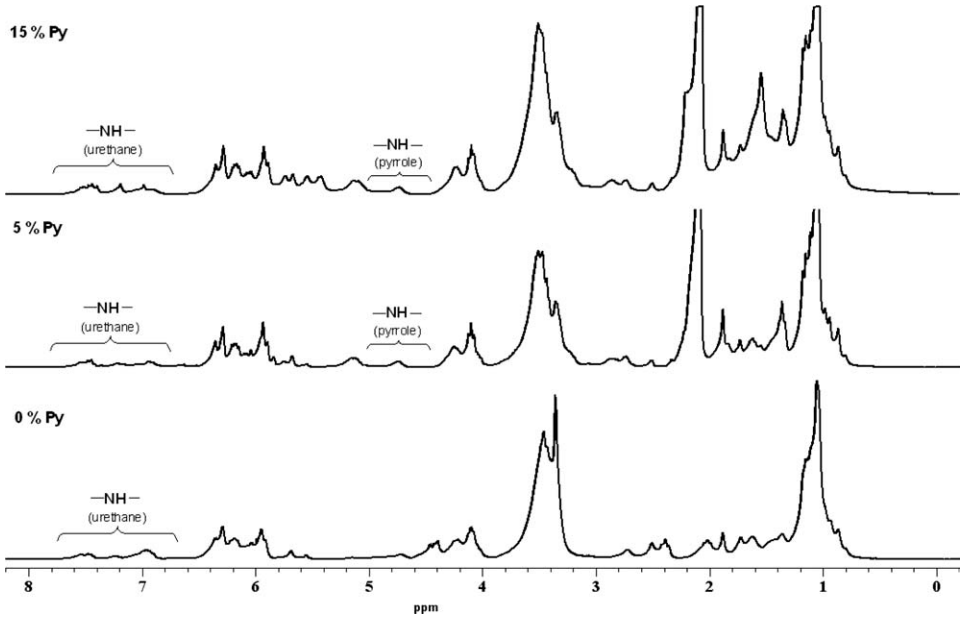

Figure 5. ^{1}H-NMR spectrum of PPy–UA with (5% Py, 15% Py) and without PPy.

$$\log \varepsilon_{\mathrm{PPy-UA}} = \log \varepsilon_{\mathrm{UA}} - q \log |(f_c - f_{\mathrm{Py\%}})/f_c|$$

$\log|(f_c - f_{\mathrm{Py\%}})/f_c| < 0$ due to the fact that $|(f_c - f_{\mathrm{Py\%}})/f_c| < 1$, so

this law predicts an increase in the dielectric constant when the PPy(f) is raised.

Furthermore, Putson et al.[43] reported that the dielectric properties of the composites depend on the volume fraction, size, and shape of components including the preparation method, interface between the conductive and nonconductive phases. In agreement with the study of Putson et al., dielectric constants were increased as a function of PPy content.

Significant reduction of dielectric constant is observed with increase in frequency for all composites (the samples with 5, 10, and 15% Py), because interfacial electric dipoles have insufficient time period to follow the variation of the electric field direction at high frequency and also due to electrode polarization effects. Kunanuruksapong and Sirivat[44] and Putson et al.[43] reported similar results in their study, and they explained that the dielectric constants decrease with increasing frequency due to the decrease of the interfacial polarization. For our composites, mechanisms of polarization depend strongly on the frequency and tend to disappear when the frequency is increased. It was found that dependences of dielectric functions on

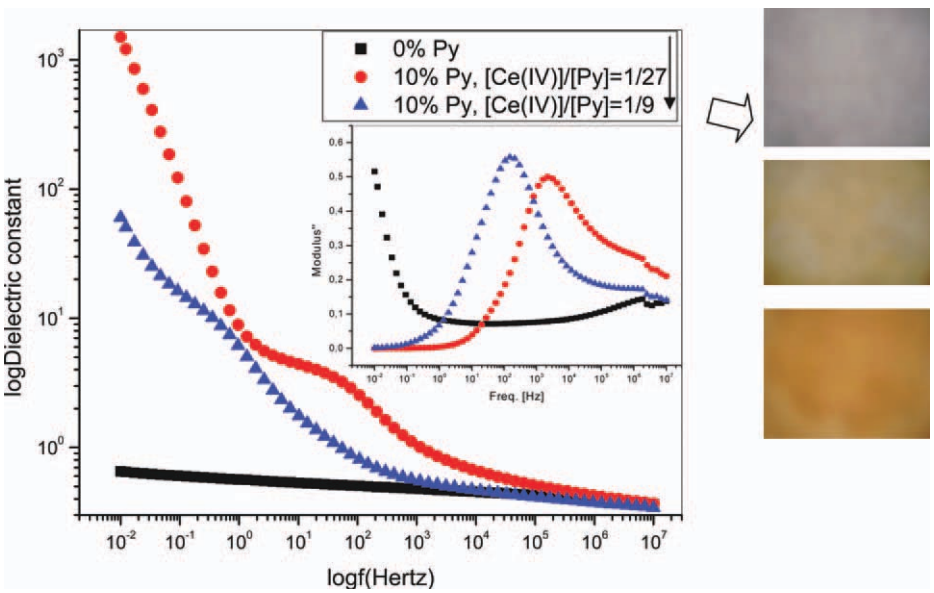

Figure 6. Dielectric constant versus frequency, inset: M'' versus frequency for the samples with different [Ce(IV)/Py] ratios. [Color figure can be viewed in the online issue, which is available at wileyonlinelibrary.com.]

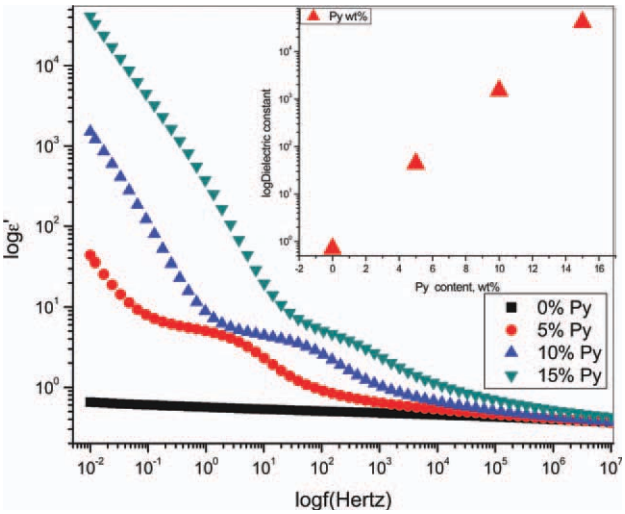

Figure 7. The plot of log ε' versus frequency (inset: an increase of dielectric constant vs. Py wt % content, at 10^{-2} Hz). [Color figure can be viewed in the online issue, which is available at wileyonlinelibrary.com.]

frequency is sensitive to the ordered state due to more or less aligned macromolecules.[45] Furthermore, It is reported[46] that the dielectric constant could be increased by a decrease in free volume and by an increase in the polarization. The more efficient chain packing and a decrease in the free volume of the polymer raise the dielectric constant. They also indicated that the presence of high polar linkages may have increased interchain electronic interactions and increased the dielectric constant and dissipation factor.[46] Our observation from Figure 7 and previous studies are proofs of incorporation of PPy in UA matrix and indicate effects of PPy on alignments of macromolecules. As a result of the dielectric study, it can also be said that incorporation of PPy leads to more aligned composites with less free volume due to high polar linkages between PPy and UA matrix. Bhadra et al.[20] prepared semiconducting composites using polyaniline (PAni) and polyolefinic thermoplastic elastomer. Dielectric properties (ε' and ε'') increased as a function of PAni content. They reported that with the increase in PAni concentration EMI SE was increased, and they concluded that this was because of the incorporation of conducting and polar filler having higher dielectric properties (ε' and ε'').[20]

The electric modulus formalism has been successfully used for the description of electrical relaxation phenomena in both microcomposites and nanocomposites. Electric modulus presentation offers advantages due to minimizing the large variation in the permittivity, loss at low frequencies and difficulties occurring from the electrode-specimen contact due to the injection of space charges and absorbed impurities.[17,47]

Figure 8 shows the real part of complex electric modulus as a function of frequency for UA matrix and PPy–UA composites. At frequencies between $\sim 10^1$ and 10^7 Hz, a sharp increase is observed for the composite samples. The inset plot of Figure 8 shows the imaginary part of complex modulus as a function of frequency. Composites exhibit a step-like transition. This transition implies the presence of relaxation processes. It becomes evident as loss peaks in the corresponding M'' versus frequency curves (inset plot of Figure 8). In the dielectric spectrum (M'' vs. frequency) of pure UA, a peak is not recorded. For all PPy–UA composite samples, the plot shows a peak at a frequency region between 10 and 10^5 Hz. This peak shifts to higher frequencies with increasing PPy content. Shifting of higher frequencies of this peak is attributed to the contribution of conductive relaxation process as indicated in the Kotp's study.[16]

The peak position of α-mode shifts to higher frequencies with the reorientation of polar segments of the polymer chain. Under the influence of an electrical field, charge carriers migrate at the interface between matrix and other constituent, forming large dipoles, while their contribution to the direct current (DC) conductivity is strongly restricted by the presence of the insulating matrix.[48] Similar result was observed for our system due to the fact that electrical characteristics of PPy and UA are

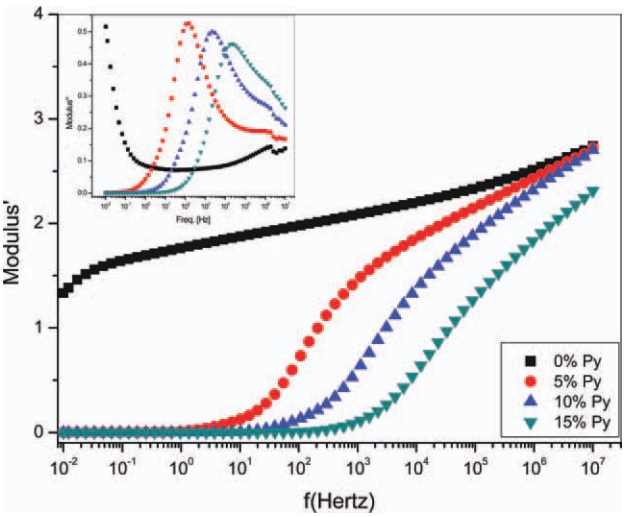

Figure 8. The plot of M' versus frequency (inset: the plot of M'' vs. frequency). [Color figure can be viewed in the online issue, which is available at wileyonlinelibrary.com.]

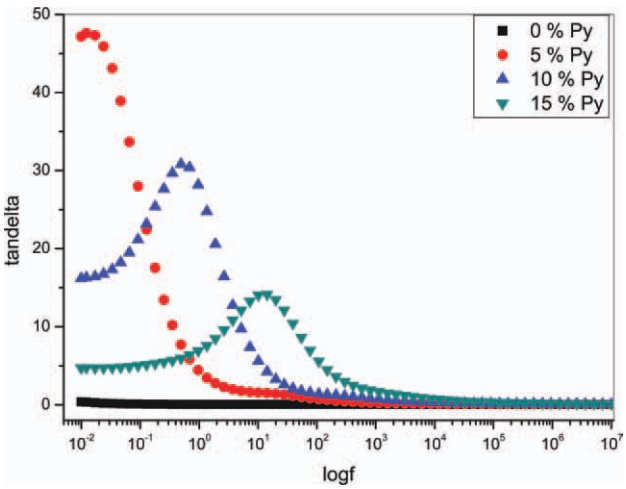

Figure 9. Tan δ values of PPy–UA composites comparing UA matrix. [Color figure can be viewed in the online issue, which is available at wileyonlinelibrary.com.]

different, and incorporation of PPy leads to arise in dielectric relaxation.

Figure 9 shows the tan δ values of PPy–UA composites comparing with UA. The loss tangent (tan δ) is a measure of the ratio of the electric energy loss to energy stored. Barick and Tripathy[34] reported that the significant enhancement in loss tangent contributes to the improvement in EMI shielding efficiency. From the observation from Figure 9, it can be said that PPy–UA composites may be used as a material for the use in EMI shielding applications.

CONCLUSIONS

In this study, our approach is to combine PPy with UA in the goal of generating a novel coating material with enhanced dielectric properties and EMI shielding efficiency. The feasibility of preparing a PPy–UA composite with a low PPy content is demonstrated, and the dielectric properties of the composites are investigated. The dielectric behavior of PPy–UA composites has been studied over a broad range of frequencies (0.01 to 10^7 Hz) and as a function of the PPy content (0–15 wt %). Experimental results show that the dielectric constants of the samples increases with an increase of PPy content. It is due to the increase of PPy content, having high dielectric molecules. For all samples, the dielectric constant decreases slowly with an increasing frequency, indicating an interfacial Maxwell–Wagner contribution to the permittivity. In addition to dielectric measurements, determinations with FTIR-ATR spectrophotometer and ^{1}H-NMR have been performed to investigate how the microstructure of the composite is affected by adding PPy in UA matrix. It is seen that PPy is blended with the UA matrix at the molecular level through H-bonding interactions. A linear relationship is also observed between the characteristic group's absorbances of PPy (from FTIR-ATR) and dielectric constant values (from dielectric spectrometer). As a result, the incorporation of PPy is very effective for enhancing the dielectric properties of UA samples and the significant enhancement in dielectric properties (dielectric constant and loss tangent) due to including PPy, contributes to the improvement in EMI shielding efficiency. So, it suggests that the polymer composites can be an alternative method for preparation of EMI shielding materials.

ACKNOWLEDGMENTS

The authors thank Prof. Dr. Ferid Salehli for measuring dielectric properties in his laboratory.

REFERENCES

1. Bouanga, C. V.; Fatyeyeva, K.; Baillif, P. Y.; Bardeau, J. F.; Khaokong, C.; Pilard, J. F.; Tabellout, M. *J. Non-Cryst. Solids* **2010,** *356*, 611.
2. Shi, G.; Rouabhia, M.; Wang, Z.; Dao, L. H.; Zhang, Z. *Biomaterials* **2004,** *25*, 2477.
3. Wang Y.; Jing, X. *Polym. Adv. Technol.* **2005,** *16*, 344.
4. Malmonge, J. A.; Santos, M. A. D.; Sakamoto, W. K. *J. Mater. Sci.* **2005,** *40*, 17, 4557.
5. Njuguna, J.; Pielichowski, K. *J. Mater. Sci.* **2004,** *39*, 4081.
6. Barde, W. S.; Pakade, S. V.; Yawale, S. P. *J. Non-Cryst. Solids* **2007,** *353*, 1460.
7. Wang, Y.; Sotzing, G. A.; Weiss, R. A. *Chem. Mater.* **2008,** *20*, 2574.
8. Patrício, P. S. O.; Cury, L. A.; Silva, G. G.; Neves, B. R. A. *Ultramicroscopy* **2008,** *108*, 302.
9. Lee, B.; Kim, H. *Polym. Degrad. Stab.* **2006,** *91*, 1025.
10. Lu, W. H.; Xua, W. J.; Wu, Y. M.; Zhou, X.; Lu, Y. B.; Xiong, Y. Q. *Progr. Org. Coat.* **2006,** *56*, 252.
11. Oprea, S. *Polym. Degrad. Stab.* **2002,** *75*, 9.
12. Larché, J. F.; Bussière, P. O.; Gardette, J. L. *Polym. Degrad. Stab.* **2011,** *96*, 1438.
13. Choi, J. S.; Seo, J.; Khan, S. B.; Jang, E. S.; Han, H. *Prog. Org. Coat.* **2011,** *71*, 110.
14. Guo, C.; Zheng, Z.; Zhu, Q.; Wang, X. *Polym.-Plast. Technol. Eng.* **2007,** *46*, 1161.
15. Sakamoto, W. K.; Kanda, D. H. F.; Andrade, F. D.; *J. Mater. Sci.* **2003,** *38*, 1465.
16. Kotp, A. E. *Int. J. Basic Appl. Sci. IJBAS-IJENS* **2010,** *10*, 28.
17. Kalini, A.; Gatos, K. G.; Karahaliou, P. K.; Georga, S. N.; Krontiras, C. A.; Psarras, G. C. *J. Polym. Sci. B: Polym. Phys.* **2010,** *48*, 2346.
18. Chung, D. D. L. *Carbon* **2001,** *39*, 279.
19. Li, N.; Huang, Y.; Du, F.; He, X.; Lin, X.; Gao, H.; Ma, Y.; Li, F.; Chen, Y.; Eklund, P. C. *Nano Lett.* **2006,** *6*, 1141.
20. Bhadra, S.; Singha, N. K.; Khastgir, D. *Curr. Appl. Phys.* **2009,** *9*, 396.
21. Lee, C. Y.; Song, H. G.; Jang, K. S.; Oh, E. J.; Epstein, A. J.; Joo, J. *Synth. Met.* **1999,** *102*, 1346.
22. Ahmad, K.; Pan, W.; Shi, S. L. *Appl. Phys. Lett.* **2006,** *89*, 133122.
23. Yanilmaz, M.; Kalaoglu, F.; Karakas, H.; Sarac, A. S. *J. Appl. Polym. Sci.,* **2012**, *125*, 4100.
24. Yanilmaz, M.; Kalaoglu, F.; Karakas, H.; Sarac, A. S. *J. Textile Apparel* **2011,** *21*, 3.
25. Yen, M. S.; Huang, C. N.; Hong, P. D. *Polym. Comp.* **2008,** *29*, 45.
26. Lin, Y. H.; Liao, K. H.; Chou, N. K.; Wang, S. S.; Chu, S. H.; Hsieh, K. H. *Eur. Polym. J.* **2008,** *44*, 2927.
27. Xu, H.; Qiu, F.; Wang, Y.; Wu, W.; Yang, D.; Guo, Q. *Prog. Org. Coat.* **2012,** *73*, 47.
28. Fang, S.; Gao, L.; Zhou, L.; Zheng, Z.; Guo, B.; Zhang, C. *J. Appl. Polym. Sci.* **2009,** *111*, 724.
29. Katarzyna, M. S.; Gouma, P. *J. Nanopart. Res.* **2006,** *8*, 769.
30. Dallas, P.; Niarchos, D.; Vrbanic, D.; Boukos, N.; Pejovnik, S.; Trapalis, C.; Petridis, D. *Polymer* **2007,** *48*, 3162.
31. Babu, K. F.; Senthilkumar, R.; Noel, M.; Kulandainathan, M. A.; *Synth. Met.* **2009,** *159*, 1353.
32. Yilgor, E.; Burgaz, E.; Yurtsever, E.; Yilgor, I. *Polymer* **2000,** *41*, 849.
33. Oprea, S.; Vlad, S.; Stanciu, A.; Ciobanu, C.; Macoveanu, M. *Eur. Polym. J.* **1999,** *35*, 1269.

34. Barick, A. K.; Tripathy, D. K. *Composites: Part A* **2010,** *41*, 1471.

35. Barick, A. K.; Tripathy, D. K. *Mater. Sci. Eng.* **2011,** *B176*, 1435.

36. Sung, P. S. C.; Schneider, S. N. *Macromolecules* **1975,** *8*, 68.

37. Lu, W. H.; Xu, W. J.; Wu, Y. M.; Zhoua, X.; Lu, Y. B.; Xiong Y. Q. *Prog. Org. Coat.* **2006,** *56*, 252.

38. Oprea, S.; Vlad, S.; Stanciu, A.; Macoveanu, M. *Eur. Polym. J.* **2000,** *36*, 373.

39. Elsayed A. H.; Haffz, A. M., *Egypt. J. Solids* **2005,** *28*, 53.

40. Tsonos, C.; Apekis, L.; Viras, K.; Stepanenko, L.; Karabanova, L.; Sergeeva, L. *Solid State Ionics* **2001,** *143*, 229.

41. Omastová, M.; Mosnáčková, K.; Trchová, M.; Konyushenko, E. N.; Stejskal, J.; Fedorko, P.; Prokeš, J. *Synth. Met.* **2010,** *160*, 701.

42. Hedvig, P. Dielectric Spectroscopy in Polymers; Adam Hilger: Bristol, **1977,** p 283.

43. Putson, C.; Lebrun, L.; Guyomar, D.; Muensit, N.; Cottinet, P. J.; Seveyrat, L.; Guiffard, B. *J. Appl. Phys.* **2011,** *109*, 024104; doi: 10.1063/1.3534000.

44. Kunanuruksapong, R.; Sirivat, A. *Curr. Appl. Phys.* **2011,** *11*, 393.

45. Valentová, H.; Nedbal, J.; Ilavský, M.; Pissis, P.; *Polymer* **2005,** *46*, 4175.

46. Hwang, H. J.; Li, C. H.; Wang, C. S. *J. Appl. Polym. Sci.* **2005,** *96*, 2079.

47. Psarras, G. C.; Gatos, K. G.; Karahaliou, P. K.; Georga, S. N.; Krontiras, C. A.; Karger-Kocsis, J. *Expr. Polym. Lett.* **2007,** *1*, 837.

48. Liu, J.; Duan, C. G.; Yin, W. G.; Mei, W. N.; Smith, R. W.; Hardy, J. R. *Phys. Rev.* **2004,** *70*, 144106.